



Toroidal rotation as an explanation for plasma flow observations in the Alcator C-Mod scrape-off layer [☆]

B. LaBombard ^{a,*}, S. Gangadhara ^a, B. Lipschultz ^a, C.S. Pitcher ^b

^a Plasma Science and Fusion Center, Massachusetts Institute of Technology, Room NW17-109, 175 Albany Street, Cambridge, MA 02139, USA

^b Institute for Aerospace Studies, University of Toronto, 4925 Dufferin Street, Toronto, Canada, M3H 5T6

Abstract

Parallel and $\underline{E} \times \underline{B}$ plasma flows near the separatrix on the outside midplane of Alcator C-Mod are investigated with a scanning probe for a range plasma densities, currents, and magnetic fields. Strong parallel flows (up to Mach 0.6) are found to peak ~ 2 mm into the scrape-off layer (SOL), reverse nearly symmetrically with magnetic field reversal, and decrease in magnitude with increasing line-averaged density normalized to the Greenwald density. $\underline{E} \times \underline{B}$ flows in the SOL inferred from the poloidal propagation velocity of plasma fluctuations appear to compensate these parallel flows and scale similarly, i.e., the dominant flow pattern is a pure toroidal rotation. $\underline{E} \times \underline{B}$ flows inferred by probe-sheath potentials are generally smaller, exhibit more scatter, and do not scale the same, perhaps indicating a less reliable measurement. These measurements suggest a residual poloidal flow (along field lines) of ~ 0.2 to ~ 1 times the electron diamagnetic velocity, depending on plasma conditions.

© 2003 Elsevier Science B.V. All rights reserved.

PACS: 52.40.Hf; 52.70.Ds; 52.70.Nc

Keywords: Plasma flow; Mach probe; Toroidal rotation; $\underline{E} \times \underline{B}$ flow; Fluctuation phase velocity

1. Introduction

Plasma flow along magnetic field lines approaching a fraction of the plasma sound speed has been seen in scrape-off layer (SOL) regions far from material surfaces in many tokamaks [1–6]. There is renewed interest in identifying the drive mechanisms since the flows may affect impurity retention in the divertor, impurity transport in the SOL, and the balance of impurity erosion and redeposition between inner and outer divertor surfaces.

Parallel flows above the outer divertor in Alcator C-Mod were reported previously [4]. Near the separatrix, the flow was directed towards or away from the divertor

entrance, depending on the plasma current and toroidal magnetic field direction. These sometimes ‘reversed flows’ appeared to circulate the plasma poloidally, suggesting that an asymmetry in divertor ionization may be partly responsible. Possible roles of divertor ionization imbalance and/or poloidal variations in cross-field transport in driving parallel flows in C-Mod are presently being examined [7]. Measurements and modeling in DITE [8], JT-60U [5], and JET [9] indicate that flows can arise from toroidal effects such as Pfirsch–Schulter currents, ballooning transport, and co-current toroidal momentum generation. Biasing experiments in TdeV [3] showed that the plasma tends to rotate toroidally in response to an imposed radial electric field. This response is intuitive: it is a divergence-free motion incurring minimal resistance in the axisymmetric geometry. It also does not result in net poloidal plasma or impurity flows.

In this paper, probe measurements of flow near the outside midplane on Alcator C-Mod are assembled to

[☆] Paper presented at the 15th PSI conference, Gifu, Japan, 27–31 May 2002.

* Corresponding author. Tel.: +1-617 253 7264; fax: +1-617 253 0627.

E-mail address: labombard@psfc.mit.edu (B. LaBombard).

address the question: does toroidal rotation simply explain the observed plasma flow or are other mechanisms playing a role? The outside midplane appears to be an ideal location for addressing this question since flows driven from ionization imbalance and poloidal variation in cross-field transport tend to exhibit a stagnation point there [7]. Parallel flow is inferred by a Mach probe while $\underline{E} \times \underline{B}$ flows are obtained from two methods: the propagation velocity of plasma fluctuations and radial electric field from sheath potentials.

2. Experiment

A cross-section of a typical Alcator C-Mod equilibrium and the location of a horizontally scanning probe is shown in Fig. 1. Results are reported from ohmic heated deuterium discharges with plasma currents (I_p) between 0.5 and 1.0 MA, toroidal magnetic field strength (B_T) between 4 and 6 T, and line-averaged plasma densities, $0.8 < \bar{n}_e < 2.4 \times 10^{20} \text{ m}^{-3}$. Discharges with ‘normal’ B_T and I_p direction ($B \times \nabla B$ towards lower x-pt) and reversed B_T and I_p direction are included. In all cases, the plasma had a lower single-null magnetic equilibrium, similar to that shown in Fig. 1, with I_p in the direction of B_T .

A close-up view of the horizontal-scanning probe head, located 10 cm above the outer midplane, is shown in Fig. 1. The East and West electrodes sample plasma from opposite directions along the same field line,

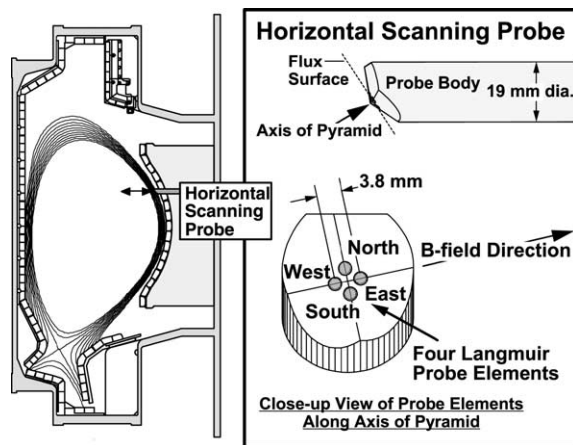


Fig. 1. Parallel and cross-field flow data are recorded by a horizontal scanning probe located 10 cm above the outer midplane. The probe head employs four tungsten electrodes (1.5 mm dia.), equally spaced around the apex of a molybdenum pyramid and machined to match its surfaces. The North and South probes record the poloidal dispersion of floating potential fluctuations while the East and West probes are operated in a swept-voltage mode, yielding density, electron temperature and parallel flow velocity information.

forming a ‘Mach probe pair’ in which the parallel Mach number can be estimated from the ratio of ion saturation currents, $M_{\parallel} = 0.43 \ln(I_{\text{east}}/I_{\text{west}})$ [10]. By fitting positive and negative-going I - V characteristics from the East and West electrodes, densities, temperatures, and parallel Mach numbers along the probe’s trajectory are obtained every 0.25 ms (corresponding to ~ 0.25 mm of probe travel). The North and South electrodes were operated in a floating-voltage mode (1 MHz sample frequency). All data is mapped along flux surfaces to the distance outside the separatrix at the plasma midplane, ρ . Using SOL power balance and electron pressure mapping constraints, the location of the separatrix is determined to an accuracy of ~ 2 mm.

3. Plasma profiles and estimates of flow velocities

Density, electron temperature, floating potential, and parallel plasma flow velocity profiles are shown in Fig. 2 for a set of representative discharges. The symbol-marked curves are smooth spline fits to the many data points that are generated over the probe’s trajectory. Parallel flow velocities (V_{\parallel}) are computed using the Hutchinson formulation [10] and an estimate of the local plasma sound speed with $T_i \approx T_e$. This formulation assumes the ratio of particle to momentum diffusivities to

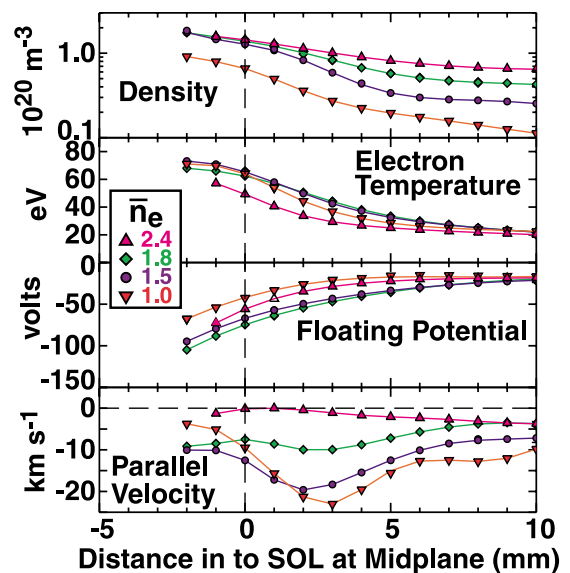


Fig. 2. Representative profiles of density, electron temperature, floating potential, and parallel flow velocity are shown. Discharge conditions are: ohmic L-mode with $I_p = 0.8$ MA and $B_T = 5.3$ T (normal directions). Line-averaged density in units of 10^{20} m^{-3} is indicated by the different symbols. All data are plotted versus distance into the SOL, mapped to the outer midplane.

be unity; varying this ratio by a factor of two leads to a 20% variation in the inferred parallel flow velocities. Negative values of V_{\parallel} correspond to flow directed from outer to inner divertor surfaces.

As seen in Fig. 2, parallel flows in the SOL can be quite large; inferred values up to Mach 0.6 are routinely found at a location $\sim 2\text{--}3$ mm outside the separatrix in low density discharges. The V_{\parallel} profile peaks outside the separatrix region, implying that V_{\parallel} is generated within the SOL region itself. Fig. 2 shows the evolution of the V_{\parallel} profile with plasma density. As the plasma density is raised the magnitude of the flow decreases across the profile.

Two different estimates are made for the cross-field plasma velocity, $v_{E \times B}$, one from the poloidal propagation of plasma fluctuations and one from the radial gradient in the inferred plasma potential profile. The poloidal phase velocity of plasma fluctuations can be computed from the North and South floating potential data. A standard analysis is employed here in which the frequency and poloidal wave number-resolved fluctuation power spectrum, $S(k, \omega)$, is deduced by a two-point correlation method [11]. In general, $S(k, \omega)$ is found to exhibit an elliptical shape in the (k, ω) plane, with minor axis much smaller than major axis. The slope of major axis of the ellipse is found by minimizing the $S(k, \omega)$ -weighted ‘moment of inertia’ about that axis. This slope, which is the power-averaged poloidal phase velocity of the plasma fluctuations, v_{ph} , is found to be reliably identified with a standard deviation of less than 20% for data taken over the SOL region $\rho \leq 6$ mm.

It is well established that fluctuations in the edge plasma propagate with a superposition of $\underline{E} \times \underline{B}$ and drift-wave velocities,

$$v_{ph} = v_{E \times B} + v_d; \quad v_d \approx \frac{T_e}{B} \frac{\nabla_r n}{n} + \alpha \frac{\nabla_r T_e}{B}. \quad (1)$$

The parameter, α , accounts for the contribution to v_d due to finite electron temperature fluctuations and is of order $\sim \bar{T}_e n / \bar{n} T_e$. Experiments [12,13] and modeling [14,15] indicate that this parameter is near unity in the edge plasma. In the present paper, separate $v_{E \times B}$ profiles are computed from Eq. (1) with $\alpha = 0$ and $\alpha = 1$ to explore the sensitivity to this parameter. Positive values of $v_{E \times B}$ are directed from inner to outer divertor surfaces.

From the electron temperature and floating potential profiles, V_f , the plasma potential and corresponding $v_{E \times B}$ can be estimated from a probe-sheath model,

$$\Phi = V_f + \delta T_e; \quad v_{E \times B} = -\frac{\nabla_r (V_f + \delta T_e)}{B}. \quad (2)$$

Parameter, δ , characterizes the sheath potential drop. For a pure deuterium plasma with Maxwellian electrons and no secondary electron emission (ion-induced, electron-induced, or thermionic), $\delta \approx 2.8$. For the present paper, a correction to δ is included, accounting for

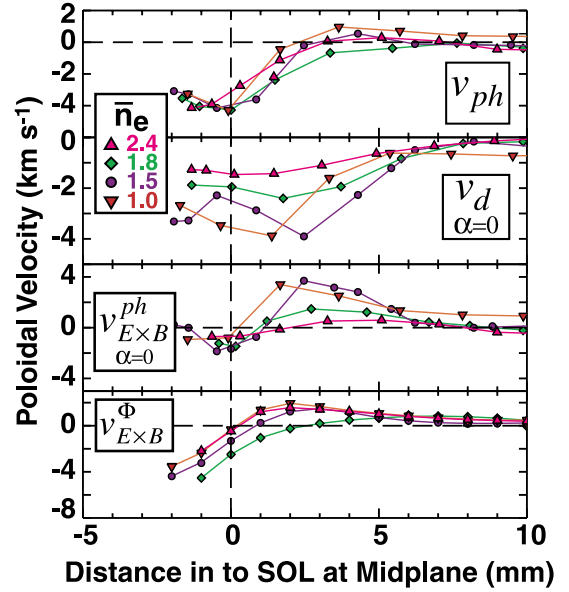


Fig. 3. Profiles of plasma fluctuation phase velocity (v_{ph}), drift-wave propagation velocity (v_d) and inferred $\underline{E} \times \underline{B}$ velocity ($v_{E \times B}^{ph}$) (from Eq. (1) with $\alpha = 0$), and $\underline{E} \times \underline{B}$ velocity inferred from probe-sheath model ($v_{E \times B}^{\phi}$) (Eq. (2)). The discharges correspond to those shown in Fig. 2. $v_{E \times B}^{ph}$ and $v_{E \times B}^{\phi}$ exhibit quantitative differences; $v_{E \times B}^{ph}$ varies strongly with discharge density while $v_{E \times B}^{\phi}$ does not.

electron-induced secondary electron emission from tungsten with a primary electron population at temperature T_e .

Fig. 3 shows profiles of v_{ph} , v_d and $v_{E \times B}^{ph}$ (Eq. (1) with $\alpha = 0$), and $v_{E \times B}^{\phi}$ (Eq. (2)) obtained for the discharges of Fig. 2. Although both estimates show qualitatively similar profiles, the magnitudes and trends with discharge conditions are different. Values of $v_{E \times B}^{ph}$ are generally more positive than $v_{E \times B}^{\phi}$ and are a factor of two higher near $\rho \sim 2$ mm, despite the fact that $v_{E \times B}^{ph}$ has been computed with $\alpha = 0$. Also $v_{E \times B}^{ph}$ exhibits a systematic dependence on discharge conditions, particularly near $\rho \sim 2$ mm, while $v_{E \times B}^{\phi}$ does not.

These differences prompt us to consider the accuracy of the inferred $v_{E \times B}$ values; both methods involve taking the difference in two quantities that have some inherent uncertainty. The probe-sheath method requires: (1) a reliable model of the sheath potential drop, δ , in the presence of possible non-thermal electron effects and possible thermionic electron emission, and (2) accurate measurements of the local floating potential. A complexity arises in determining the floating potential in a flowing plasma; an ‘upstream’ probe will have a higher floating potential (owing to higher density, plasma potential) than a downstream probe with all other parameters being equal. In view of these difficulties, the fluctuation phase velocity method appears to have an

advantage; it is insensitive to surface physics effects. Although the method does require knowledge of α , $\alpha = 0$ should yield a reliable lower-bound estimate of $v_{E \times B}$.

4. Comparison of parallel and poloidal flow velocities in SOL

Comparing the parallel flows in Fig. 2 with the $v_{E \times B}$ flows in Fig. 3, one can see that they tend to have the opposite sign in the SOL, i.e., the poloidal components of these flows tend to cancel. In order to explore this behavior in more detail, data from a wider range of plasma conditions were assembled: 144 profiles with normal magnetic field direction and 81 profiles with reversed. For both field directions, current, field and density scans were performed: $0.5 < I_p < 1.0$ MA, $4 < B_T < 6$ T, $0.8 < \bar{n}_e < 2.4 \times 10^{20}$ m⁻³.

Fig. 4 shows the full set of parallel and poloidal flow velocity profiles. The parallel flow is seen to have a nearly symmetric behavior with respect to magnetic field direction: Mach number profiles peak in the range $\rho \sim 2\text{--}3$ mm and have largest magnitudes of around 0.6.

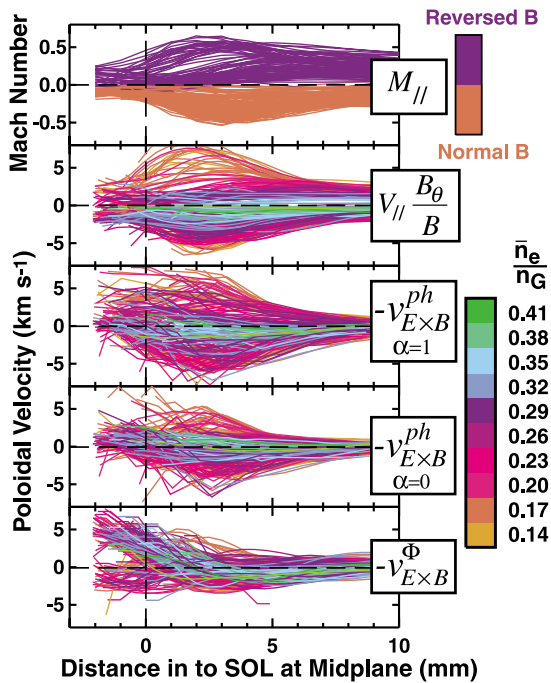


Fig. 4. Plasma velocity profiles inferred from 144 probe scans are overlaid: parallel Mach number, poloidal projection of parallel flow velocity, and three computations of $-v_{E \times B}$ from Eqs. (1) and (2). Profiles in the first panel are color-coded according to B -field direction. Profiles in the remaining panels are colored according to \bar{n}_e/n_G .

The second panel shows the poloidal projection of the local parallel flow velocity, while the remaining panels show the negative of $v_{E \times B}$ from three computations: Eq. (1) with $\alpha = 0$ and $\alpha = 1$, and Eq. (2). Curves in the last four panels are colored according to line-average discharge density normalized to the Greenwald density, \bar{n}_e/n_G . (This parameter was chosen because edge plasma profiles and local transport conditions correlate with this quantity [16].) If $B_\theta v_{||}/B$ and $v_{E \times B}$ were to exactly cancel over all plasma conditions then those panels would look identical. Although not identical, the panels containing $B_\theta v_{||}/B$ and $-v_{E \times B}^{ph}(\alpha = 1)$ are remarkably alike, exhibiting: (1) reversal in flow direction with B_T reversal, (2) similar magnitude and profile shapes, peaking in the range $\rho \sim 2\text{--}3$ mm, and (3) similar dependence on \bar{n}_e/n_G , favoring smaller flow velocities at large \bar{n}_e/n_G .

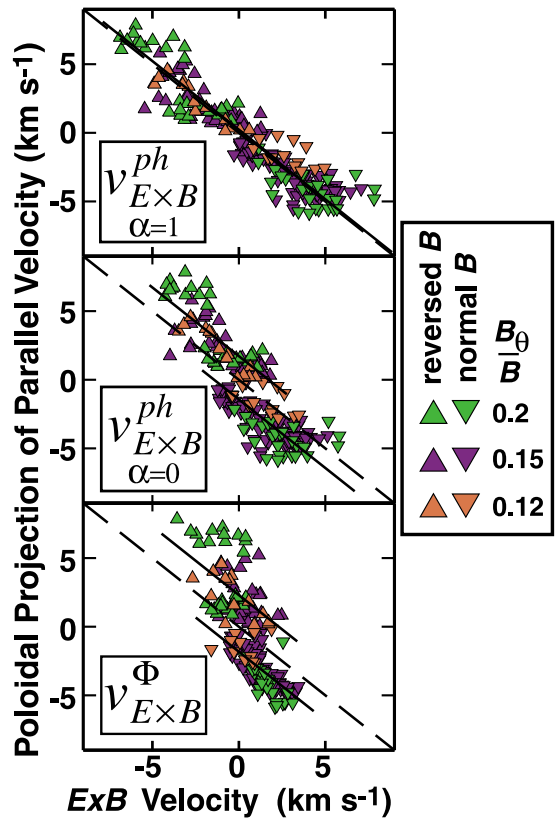


Fig. 5. The poloidal projection of parallel plasma flow velocity is plotted versus three computations of $\underline{E} \times \underline{B}$ velocity at a location 3 mm into the SOL: $\underline{E} \times \underline{B}$ velocity from fluctuation phase velocity (Eq. (1) with $\alpha = 0$ and $\alpha = 1$), and probe-sheath potential (Eq. (2)). Data are grouped by symbol color according to ratio of poloidal to total magnetic field at the probe location. The poloidal projection of parallel plasma flow velocity (top panel) is found to track remarkably well the $\underline{E} \times \underline{B}$ velocity inferred from plasma fluctuations ($\alpha = 1$).

Owing to the plasma current and toroidal field scans, B_θ/B at the scanning probe location was changed by a factor of ~ 2 . An important question is: as $v_{E \times B}$ varies with \bar{n}_e/n_G , does $B_\theta v_\parallel/B$ vary proportionally for all B_θ/B values? Fig. 5 shows $B_\theta v_\parallel/B$ plotted versus three computations of $v_{E \times B}$ at the location $\rho = 3$ mm. In each panel, the horizontal and vertical axes are the same; any data falling on the dashed line would correspond to a net zero velocity in the poloidal direction. Solid black lines are drawn through the centroids of each cluster of normal or reversed B_T data points and parallel to the dashed lines. As seen in the first panel, $B_\theta v_\parallel/B$ is found to track remarkably well with $v_{E \times B}^{\text{ph}} (\alpha = 1)$, independent of the value of B_θ/B . On the other hand, $B_\theta v_\parallel/B$ does not track so well with $v_{E \times B}^\phi$. By this measure, a residual poloidal flow of ~ 0.2 to 1 times the electron diamagnetic velocity (depending on plasma conditions) is suggested.

5. Conclusions

Parallel flows up to Mach 0.6 are measured near the outer midplane on Alcator C-Mod that peak ~ 2 mm into the SOL, reverse nearly symmetrically with magnetic field, and decrease in magnitude with increasing \bar{n}_e/n_G . In contrast, modeling suggests that flows driven by ionization and cross-field particle transport alone lead to a nearly stagnant parallel flow profile on the outer midplane [7]. Based on the poloidal propagation velocity of fluctuations, the parallel flows in the SOL appear to be compensated by $\underline{E} \times \underline{B}$ flows that scale similarly, i.e., the overall flow pattern is nearly a pure toroidal rotation. $\underline{E} \times \underline{B}$ flows estimated from sheath potentials are found to be smaller in magnitude, scale

differently with plasma conditions, and only partially compensate the parallel flows. By this measure, a residual poloidal flow (along field lines) of ~ 0.2 to ~ 1 times the electron diamagnetic velocity is indicated, depending on plasma conditions.

Acknowledgement

This work is supported by US D.o.E. Coop. Agreement DE-FC02-99ER54512.

References

- [1] V.A. Vershkov, S.A. Grashin, A.V. Chankin, J. Nucl. Mater. 145 (1987) 611.
- [2] R.A. Pitts, G. Vayakis, G.F. Matthews, V.A. Vershkov, J. Nucl. Mater. 176 (1990) 893.
- [3] C.S. MacLachy et al., J. Nucl. Mater. 196 (1992) 248.
- [4] B. LaBombard et al., J. Nucl. Mater. 241–243 (1997) 149.
- [5] N. Asakura et al., Nucl. Fusion 39 (1999) 1983.
- [6] S.K. Erents, A.V. Chankin, G.F. Matthews, P.C. Stangeby, Plasma Phys. Controlled Fusion 42 (2000) 905.
- [7] C.S. Pitcher, these Proceedings.
- [8] J. Hugill, J. Nucl. Mater. 196 (1992) 918.
- [9] A.V. Chankin et al., J. Nucl. Mater. 290 (2001) 518.
- [10] I.H. Hutchinson, Phys. Rev. A 37 (1988) 4358.
- [11] J.M. Beall, Y.C. Kim, E.J. Powers, J. Appl. Phys. 53 (1982) 3933.
- [12] M.A. Meier, R.D. Bengtson, G.A. Hallock, A.J. Wootton, Phys. Rev. Lett. 87 (2001) 085003.
- [13] J.A. Boedo et al., Phys. Plasmas 8 (2001) 4826.
- [14] S.J. Zweben et al., Phys. Plasmas 9 (2002) 1981.
- [15] K. Hallatschek, private communication.
- [16] B. LaBombard et al., Phys. Plasmas 8 (2001) 2107.